Generalised scalar-tensor theories of gravity and pressure profiles of galaxy clusters

Balakrishna S. Haridasu[1,2,3,*], *Purnendu* Karmakar[4], *Marco* De Petris[4,5,6], *Vincenzo F.* Cardone[5,6], and *Roberto* Maoli[4,5]

[1]SISSA-International School for Advanced Studies, Via Bonomea 265, 34136 Trieste, Italy
[2]INFN, Sezione di Trieste, Via Valerio 2, I-34127 Trieste, Italy
[3]IFPU, Institute for Fundamental Physics of the Universe, via Beirut 2, 34151 Trieste, Italy
[4]Dipartimento di Fisica, Sapienza Universitá di Roma, P.le Aldo Moro 2, 00185, Roma, Italy
[5]INAF - Osservatorio Astronomico di Roma, Via Frascati 33, 00040, Monteporzio Catone, Roma, Italy
[6]INFN- Sezione di Roma 1, P.le Aldo Moro 2, 00185, Roma, Italy

Abstract. In the current proceedings, we summarise the results presented during the mm Universe@NIKA2 conference, taken from our main results in [1]. We test the Degenerate higher-order scalar-tensor(DHOST) theory as a generalised platform for scalar-tensor theory at galaxy cluster scales to predict in such static systems small scale modification to the gravitational potential. DHOST theory is not only a good alternative to ΛCDM for the background evolution but also predicts small-scale modification to the gravitational potential in static systems such as galaxy clusters. With a sample of 12 clusters with accurate X-ray Intra Cluster Medium (ICM) data (X-COP project) and Sunyaev-Zel'dovich (SZ) ICM pressure (Planck satellite), we place preliminary constraints on the DHOST parameter (Ξ_1) defining the deviation from GR. Moreover, we also collect a few supplementary analyses we have performed during the course: i) Gaussian process reconstruction without parametric assumptions, ii) $P_{\rm SZ}$-only data analysis not aided by the X-ray data. Finally, we present possible extensions to the current work which may benefit from future high sensitivity and spatial resolution observations.

1 Introduction

Einstein developed the standard general relativity (GR) by considering gravity as warps and curves in the fabric of geometric space-time, and that geometry of space-time is described only by a metric. GR can explain the majority of the cosmological observations, and requires a cosmological constant to explain the acceleration in the cosmological distance, which is however phenomenological. Therefore, if we plan to keep the basic metric structure because of the large success of GR, and add one scalar degrees of freedom to explain the acceleration, then the degenerate higher-order scalar-tensor (DHOST) theory is the best possible platform to test the largest classes of scalar-tensor theories [2, 3].

The additional degree of freedom must be suppressed at small scales by a screening mechanism to fit with the observations [4]. The radial derivative of modified Newtonian potential for the DHOST theory in the galaxy cluster, which produces the gravitational waves propagating at the velocity of light ($c_g = c$), is

*e-mail: sandeep.haridasu@sissa.it

$$\frac{d\Phi(r)}{dr} = \frac{G_{\rm N}^{\rm eff} M_{\rm HSE}(r)}{r^2} + \Xi_1 G_{\rm N}^{\rm eff} \frac{d^2 M_{\rm HSE}(r)}{dr^2}\,, \tag{1}$$

while assuming the hydrostatic equilibrium (HSE), where $M_{\rm HSE}(r)$ is the total mass within the radial distance r. Both, Ξ_1 and $G_{\rm N}^{\rm eff}$ parameters track the departure of DHOST theory from GR, which modify the ICM thermal pressure profile as

$$P^{\rm th}(r) = P^{\rm th}(0) - \int_0^r \rho_{\rm gas}(\tilde{r}) \frac{d\Phi(\tilde{r})}{dr} {\rm d}\tilde{r}\,, \tag{2}$$

where $\rho_{\rm gas}(r)$ is the gas density. Our formalism is a straight-up implementation of the so called *forward*-method, where the pressure profile is computed while assuming empirical profiles for the mass, $M_{\rm HSE}(r)$, and the electron density, $n_e(r)$, radial profiles which in our case are the standard NFW [5] and simplified Vikhlinin parametric model [6], respectively. Vikhlinin profile provides a more general parametric model in comparison to the β or the double β profiles and we also validate that the former produces variation from the multiscale fitting in [7], of no more than $\sim 5\%$ for the $n_e(r)$. In this context, several previous works have implemented similar approach either using stacked clusters and/or having complementary weak lensing data [8–10].

Throughout the current discourse we assume $H_0 = 70$ km/s Mpc^{-1}and $\Omega_{\rm m} = 0.3$. R_{500} and M_{500} carry usual definitions, i.e, total mass M_Δ within the radius R_Δ, with a mean mass density Δ times the critical density ($\rho_{\rm c}(z) = 3H^2(z)/8\pi G_{\rm N}^{\rm eff}$). Here $G_{\rm N}^{\rm eff} = \tilde{\gamma}_{\rm N} G_{\rm N}$, which represents the running of the Planck mass on large scales.

2 Main Results

Firstly, we figure that only 8 clusters out of the 12 available clusters in the dataset prefer the NFW mass profile in a comparison through information criteria (see Fig 2, of [7]). We refer to the other 4 clusters (A644, A1644, A2319 and A2255) as non-NFW clusters for brevity. As a consequence of which, we find that the non-NFW clusters fit the data within the DHOST scenario with statistical preferences reaching $\Delta \log(\mathcal{B}) >> 25$ (further details in [1] and [7]), which imply a very high preference yet providing very low values of the parameter Ξ_1, in complete disagreement with the theoretical limits [11–13]. In Figure 1, we show the fits of the GR and DHOST scenarios for A644 (non-NFW) and A1795 cluster and the 1σ dispersion to provide a comparison. We show the posteriors for Ξ_1 obtained using the individual cluster and the joint constraint in left panel of Figure 2 and a comparison with earlier constraints in the right panel.

As the main result of our analysis we updated the limits on the modified gravity parameter $\Xi_1 = -0.030 \pm 0.043$, which is a much more stringent constrain in comparison to the earlier result of $\Xi_1 \sim -0.028^{+0.23}_{-0.17}$, reported in [8] using a similar formalism with stacked X-ray cluster profile. In a more conservative case where we utilise only 4 clusters (A1795, A3158, RXC1825 and ZW1215) having mass estimates consistent with [7], we find a less stringent $\Xi_1 = -0.061 \pm 0.074$, yet twice as tighter constraint than the earlier analysis. These 4 conservative clusters are restricted within a redshift range of $0.0597 < z < 0.0766$. In the right panel of Figure 2, we show a comparison of the earlier constraints, our results and the theoretical limits. As can be seen, our results are in excellent agreement with the latter and an improvement for the constraints on Ξ_1. The lower theoretical limit is marked by the requirement of stable static solutions of non-relativistic stars [11, 14] and the upper limits are obtained on the based on the minimum mass required for hydrogen burning in low mass red dwarfs [12, 13].

An added advantage of our current analysis is that having individual clusters spread over a redshift range of $0.04 < z < 0.1$, we are able to present for the first time the necessary

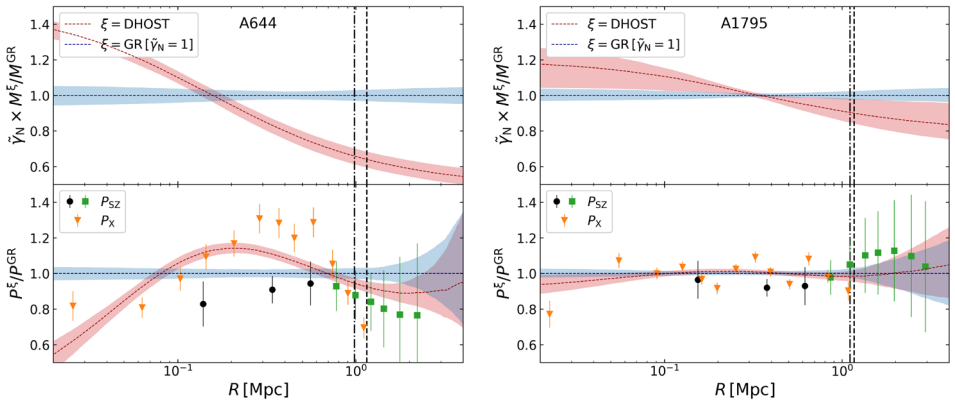

Figure 1. Mass (*upper*) and pressure (*lower*) radial profiles for the cluster A644 (*Left*) and A1795 (*Right*) in the cases of GR (blue) and DHOST (red), normalised to GR. The former cluster is an example case of the 4 non-NFW clusters, while the latter is one of the 4 clusters we retain in estimating our final conservative result. The vertical dashed (GR) and dot-dashed (DHOST) lines show R_{500}. The 3 inner P_{SZ} data points (black) are excluded in the main analysis.

assessment of time-evolution of the parameter $\Xi_1(a \equiv 1/(1+z))$. We utilise a simple first order Taylor expansion of $\Xi_1(a)$ as the scale factor, $a \to 1$ and perform a post-MCMC analysis on the inferred posteriors of the Ξ_1 obtained for individual clusters. Using 8 clusters we find a mild deviation ($\lesssim 2\sigma$) from a constant behaviour for Ξ_1, at present is however driven only by two clusters (A85 and A2142). Note however that the current redshift range used to assess possible time dependence is limited (see also [1]), and the advantage of extending the analysis over a larger dataset that covers a wider redshift range is clear.

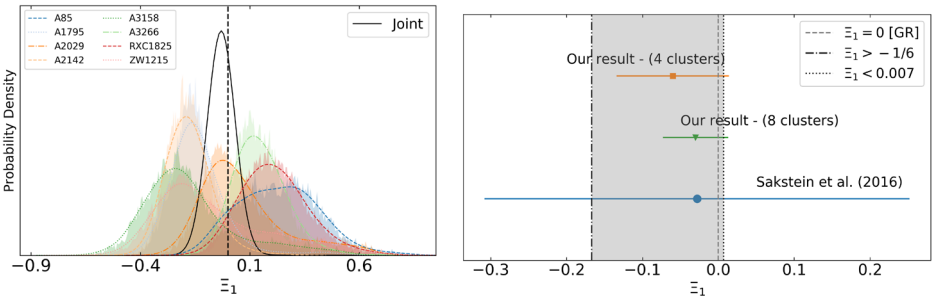

Figure 2. *Left*: Posterior distribution of the parameter Ξ_1, over-plotted by smooth Gaussian kernel density profiles. The vertical dashed line marks the GR ($\Xi_1 = 0$) case. The black curve represents our joint constraint using 8 clusters. *Right*: Constraints on the parameter Ξ_1, from an earlier analysis of 58 stacked clusters (blue) [8] and our results with 8 clusters (green) and conservative 4 clusters (orange). The grey shaded region shows the allowed region for the same parameter obtained from theoretical limits [11–13].

3 Supplementary Results

In this section we present a few supplementary analyses we have performed, also constituting possible future extension of the current work.

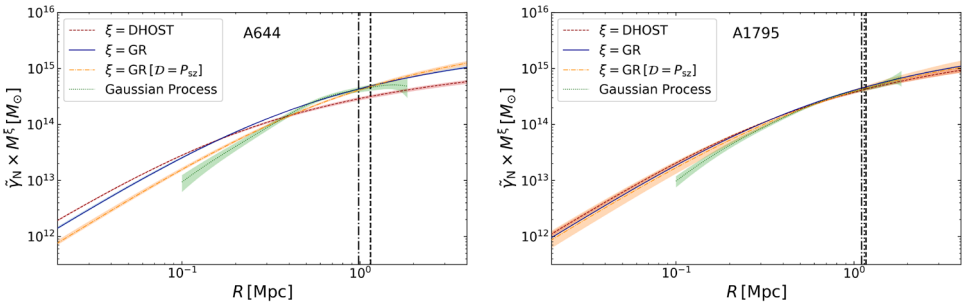

Figure 3. Mass radial profiles with 1σ dispersion for clusters A644 (*left*) and A1795 (*right*) for the GR (blue), DHOST (red) and GP (green). A644 and A1795 represent one of the non-NFW cluster and one of the 4 conservative clusters, respectively. The vertical dashed, dot-dashed and dotted lines show the R_{500} in GR, DHOST and GP, respectively. The R_{500} from the GP case coincides very well with that in GR case. The mass profiles obtained utilising only the P_{SZ} data for the GR case are shown in orange. Here the GR case corresponds to $\tilde{\gamma}_N = 1$.

3.1 Gaussian Process

In addition to the parametric analysis, we also perform a non-parametric model-independent analysis based on the Gaussian Process (GP) formalism, please see [15] and references therein for details on the method. In essence, once could reconstruct the underlying functional form $[f(x_i)]$ for a collection of Gaussian data points at $\mathbf{x} \equiv \{x_1, x_2, ..x_N\}$, assumed belonging to the same process, which now represents a GP. This is implemented by modelling a covariance $K(x_i, x_j)$, among the data points, instead of functional form for the process itself. For this purpose we independently reconstruct the electron density and the P_{SZ} pressure profiles assuming the squared-exponential (SE) [1] kernel. Note that here we cannot extrapolate the profile beyond the range of the available data, as GP tends to retrieve broad prior regions, with no constrain on the posterior. We intend the analysis with GP as an alternate verification for the fits based on the profile themselves as the model-independent method is agnostic with no assumptions made for the electron density profile and the mass profile. Therefore, a parametric method based on assumed empirical profiles is expected to serve better if it is in a good agreement with the GP method.

In Figure 3, we show the mass reconstructions obtained using the NFW profile in both the GR (blue) and DHOST (red) scenarios and the GP (green) reconstructed result. For the GP method we firstly find a lowering of the mass profile in the inner regions, which is an immediate consequence of not excluding the inner most 3 data-points of P_{SZ} data (see [7, 16]). However, being a non-parametric estimation and that it only follows the data points, we find the GP to be in better agreement towards the outskirts of the mass profile. In the case of the A644, a non-NFW cluster, we find that the model-independent reconstruction is in better agreement with the GR case than with the DHOST scenario, which is a clear indication of our results for

[1] The functional form for the SE kernel is $K(x_i, x_j) = \sigma_f^2 \exp\left[(x_i - x_j)^2/2l^2\right]$, where $\{\sigma_f, l\}$ are now free parameters inferred by optimising a log-marginal likelihood.

the latter being biased when utilising the NFW mass profile. The $R_{500} = 1.15 \pm 0.06\,[\mathrm{Mpc}]$ and $M_{500} = 4.57^{+0.73}_{-0.65}\,[10^{14}\,M_{\odot}]$ estimated using GP here are in excellent agreement with our constraints in the GR case. In the case of A1795 however, the deviation between the GR and the DHOST cases is minimal and is also reflected in the GP reconstruction. Once again the GP based $R_{500} = 1.12 \pm 0.04\,[\mathrm{Mpc}]$ and $M_{500} = 4.24^{+0.045}_{-0.040}\,[10^{14}\,M_{\odot}]$ are in excellent agreement with the parametric method assuming the NFW profile.

3.2 $P_{\rm SZ}$ only analysis

Indeed, one of the major advantages in our analysis is that we perform the joint-fit to the $T_{\rm X}$(or $P_{\rm X}$) and the $P_{\rm SZ}$ data, which provides a better estimation of the mass profile to the outskirts ($R \sim 1.2$ Mpc) of the clusters. In the screening mechanism, the GR is recovered in the innermost region of the galaxy cluster, while the gravity is gradually deviates from GR in the outskirt of the cluster. Given that, the inclusion of the $P_{\rm SZ}$ data actually provides a very suitable opportunity to asses the mass profile in a larger radial range and hence the modifications to gravity.

To contrast our constraints against the combined analysis of $P_{\rm SZ} + P_{\rm X}$, we also perform an MCMC analysis using only the $P_{\rm SZ}$ data (without excluding the 3 inner most data points). We also show the inferred mass profiles (orange) of the same in Figure 3. One can immediately notice that for the cluster A644, all the 4 contrasted scenarios are almost discordant at the face-value. This in turn indicates that a more careful assessment has to be made when combining the data sets and/or trying to assess the modifications to physics using this cluster. On the other hand, the A1795 cluster shows that all the approaches are in very good agreement, especially in the outskirts of the cluster. However, comparing the $P_{\rm SZ}$ parametric fit and the GP based reconstruction we find that the former tends to show higher masses, also in agreement with the $P_{\rm X} + P_{\rm SZ}$ analysis. The results for the posterior distributions on Ξ_1 are summarised in Appendix C. of [1].

Within the joint analysis however, one needs to check internally for a consistency between the X-ray and SZ data, see Appendix A of [16] for more details. Therefore in a similar approach we introduce an intrinsic dispersion ($\sigma_{\rm P,int}$) as a free parameter which is scaled by the modelled pressure ($\sigma_{P,\rm int} \sim P^{\rm model}\sigma_{\rm int}$) (Appendix D of [17]), added in quadrature to the error and inferred through the MCMC analysis. Alongside the dispersion, we also include a rescaling parameter η, such that $P_{\rm X}^{\rm data} \rightarrow \eta \times P_{\rm X}^{\rm data}$. We show the posterior distributions of these two consistency parameters in Figure 4 for the A644 and A1795 clusters. Clearly, both clusters show a good agreement between $P_{\rm SZ}$ and $P_{\rm X}$ data, while A644 shows a larger dispersion within the $P_{\rm X}$ data points. This in turn provides additional correlations with M_{500} and increases the error-bars, however note also that we fix $\eta = 1$ in the main analysis. Please refer to original analysis in [7, 16, 17], where these arguments are elaborated.

4 summary

As we have shown here, having the galaxy cluster physics well-mapped in a larger radial range and having several of these objects also distributed along the redshift will be crucial to assess the constraints on the Ξ_1 in individual clusters and its time evolution. We intend to explore the same with soon to be available future data. For this goal, NIKA2 SZ observations could be helpful to extend this analysis.

References

[1] B.S. Haridasu, P. Karmakar, M. De Petris, V.F. Cardone, R. Maoli (2021), 2111.01101
[2] M. Crisostomi, K. Koyama, G. Tasinato, JCAP **1604**, 044 (2016), 1602.03119

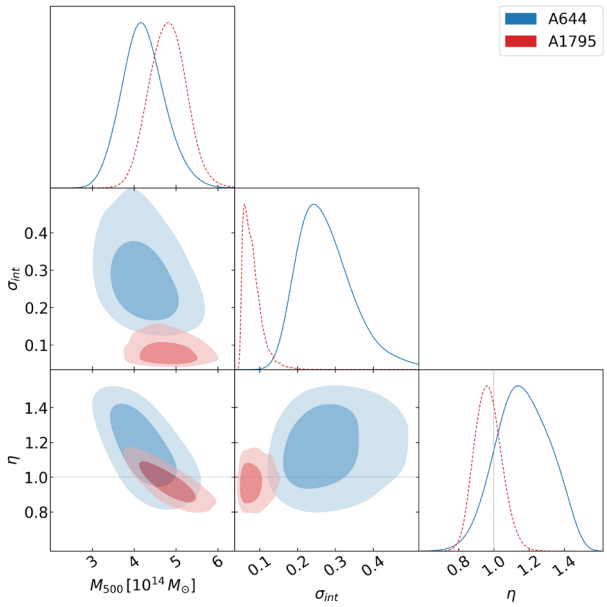

Figure 4. We compare here the posteriors for the intrinsic dispersion in the X-ray data and the scaling parameter. The dashed grey line marks the case of $\eta = 1$, which implies good agreement between the P_X and P_{SZ} data.

[3] J. Ben Achour, D. Langlois, K. Noui, Phys. Rev. **D93**, 124005 (2016), 1602.08398
[4] E. Babichev, C. Deffayet, Class. Quant. Grav. **30**, 184001 (2013), 1304.7240
[5] J.F. Navarro, C.S. Frenk, S.D.M. White, Astrophys. J. **462**, 563 (1996), astro-ph/9508025
[6] A. Vikhlinin, A. Kravtsov, W. Forman, C. Jones, M. Markevitch, S.S. Murray, L. Van Speybroeck, Astrophys. J. **640**, 691 (2006), astro-ph/0507092
[7] S. Ettori, V. Ghirardini, D. Eckert, E. Pointecouteau, F. Gastaldello, M. Sereno, M. Gaspari, S. Ghizzardi, M. Roncarelli, M. Rossetti, Astron. Astrophys. **621**, A39 (2019), 1805.00035
[8] J. Sakstein, H. Wilcox, D. Bacon, K. Koyama, R.C. Nichol, JCAP **1607**, 019 (2016), 1603.06368
[9] H. Wilcox et al., Mon. Not. Roy. Astron. Soc. **452**, 1171 (2015), 1504.03937
[10] A. Terukina, L. Lombriser, K. Yamamoto, D. Bacon, K. Koyama, R.C. Nichol, JCAP **04**, 013 (2014), 1312.5083
[11] R. Saito, D. Yamauchi, S. Mizuno, J. Gleyzes, D. Langlois, JCAP **1506**, 008 (2015), 1503.01448
[12] J. Sakstein, Phys. Rev. **D92**, 124045 (2015), 1511.01685
[13] J. Sakstein, Phys. Rev. Lett. **115**, 201101 (2015), 1510.05964
[14] I.D. Saltas, I. Sawicki, I. Lopes, JCAP **05**, 028 (2018), 1803.00541
[15] B.S. Haridasu, V.V. Lukovi´c, M. Moresco, N. Vittorio, JCAP **10**, 015 (2018), 1805.03595
[16] V. Ghirardini et al., Astron. Astrophys. **621**, A41 (2019), 1805.00042
[17] V. Ghirardini, S. Ettori, D. Eckert, S. Molendi, F. Gastaldello, E. Pointecouteau, G. Hurier, H. Bourdin, Astron. Astrophys. **614**, A7 (2018), 1708.02954